A Composite Case Study of Kinematic Vertical Motions

Tai-Jen George Chen

Dept. of Atmos. Sci., National Taiwan University, Taipei, Taiwan, ROC

(*Manuscript received 31 March 1976, in revised form 3 April 1976*)

Abstract

An analysis for the kinematical vertical motions has been carried out by using O'Brien's (1970) special adjustment technique. A composite case, including four cases of winter time polar air outbreaks, was used for present study. Detailed three-dimensional vertical velocity field together with the radar reports are presented and discussed. Results show that an area of maximum vertical motion usually located at different position in relation to the surface center in contrast to the results in different individual case studies, which did not use polar air outbreak cases, made by some other researchers.

1. Introduction

Vertical motion is one of the most important parameters in both diagnostic and prognostic studies of the atmosphere. The distribution of vertical motion has profound influence on the distribution of cloudiness and precipitation. Due to its smallness in magnitude in the large scale motions as compared to the horizontal velocity, it is not measured directly. Thus, the vertical motion is estimated indirectly from the other meteorological parameters, such as horizontal winds, temperature, and pressure. The methods commonly used have been called (1) kinematic method (e. g. Lateef 1967, Fankhauser 1969, Smith 1971), (2) adiabatic method (e. g. Lateef 1968), (3) trajectory method (e. g. Danielsen 1961, Bosart 1970), and (4) numerical method (e.g. Danard 1964, Krishnamurti 1968b).

Each method has certain inherent advantages and disadvantages. The kinematic method uses the continuity equation in pressure coordinates to obtain the vertical motion from the horizontal divergence. The primary advantage of this method lies in its mathematical simplicity and in the fact that hydrostatic balance is the only assumption. However, errors in the wind observations as well as in the computed horizontal divergence often tend to accumulate through the vertical integration. As a result, unrealistic estimates of vertical velocities are often found in the upper troposphere.

The adiabatic method has the advantage of a simple mathematical formulation, adiabatic condition is the only physical assumption. However, it possesses a limitation in application wherever diabatic effect is significant or the actual lapse rate approaches the dry adiabatic.

Trajectory method can provide the average vertical motion along the trajectories on either the isentropic surface or constant wet-bulb potential temperature surface. However, it encounters difficulty in the trajectory analysis in the area of turbulent mixing. Also, the construction of trajectory is a very time-consuming task.

The numerical method generally obtains vertical motion by solving the so-called "ω-equation" in either quasi-geostrophic or balanced model. It possesses the advantage of being not using the actual winds, and thus avoid the cumulative bias errors in the kinematic method. However, it faces a formidable task in estimating the effects from diabatic and frictional processes.

Diabatic effect contributed to the vertical motion can be significant under certain circumstances. It was found that contribution to the vertical velocity by long wave radiation in clear sky region is about 60-70% of the adiabatic value (Bullock et al 1969). Danard (1964) documented a case that the value of vertical velocity obtained from guasi-geostrophic ω-equation by neglecting the release of latent heat is only one-fourth of the value computed by the kinematic method below 600mb.

Previous studies (e. g. Lateef 1967, Fankhauser 1969, Schmidt and Johnson 1972) suggested that the reliability of the kinematic method is sufficient for use in diagnostic studies if some techinques are employed to reduce the cumulative errors. A case study by Smith (loc. cit.) indicated that the kinematic ω's are realistic as far as the observed weather is concerned. In view of the advantages and disadvantages of the various methods discussed above, the kinematic method is then adopted for the present case study. The purpose of this research is to reveal the horizontal and vertical structures of the vertical motion field in a composite case. Cases were chosen during the periods of the winter time polar air outbreaks penetration into lower latitudes. Vertical motion in relation to the surface centers of cyclones and anticyclones as well as to the radar echoes are presented and discussed.

2. Cases and Synoptic Discussions

(a) Case selection

Cases have been chosen over the North American Continent, Gulf of Mexico, Central America and Caribbean area. These areas have reasonably good coverage and quality of surface and radiosonde observations. Also, these are regions in the Northern Hemisphere where cold polar air outbreaks frequently intrude into the tropics during the winter season.

1000-500 mb thickness maps as received from the National Weather Service (NWS) over facsimile were used in the case selection for the winter season, (October through March), 1968 through 1972. The following criteria, established subjectively and arbitrarily, were used for case selection: (1) the existence of a well-defined thermal trough and its associated baroclinic zone over the Gulf of Mexico and western Caribbean and (2) the penetration of the 5700 meter thickness line south of 20°N between 85°W and 95°W. These are favorable longitudes for the penetration of cold air into the tropics from the North American Continent. Twenty-one cases were found to satisfy these criteria during the five-year period. These twenty-one cases were then checked against surface maps and satellite pictures to see if there was a polar front penetration into the Caribbean to the south of 15°N on the surface analysis and also a discernible cloud band associated with it on the satellite pictures. Sixteen of the twenty-one cases were found to meet these conditions. Of these sixteen cases, four have been chosen which have the polar fronts concentrated in a 300 km wide NE-SW-oriented band south of 30°N at the time of most pronounced equatorward

penetration of the cold air in terms of the intensity of baroclinic zone. In addition, they have the polar anticyclones and downstream cyclones located in the similar region. The choice of these four cases, two cases at 0000Z and two at 1200Z, will hopefully suppress, the diurnal variation. It is well known that diurnal variation of different meteorological parameters sometimes overwhelms the interesting synoptic-scale changes, especially in the tropics. Consequently, the composite case chosen from two cases both at 0000Z and 1200Z is believed to be more representative for a synoptic-scale system. The significance of this composite case lies in the fact that these four chosen cases has very similar characteristics at different levels at different time periods.

The dates of the four cases are as follows for eight time periods at 12-hour interval.

(a) November 10, 1968, 1200Z to 14, 0000Z
(b) February 7, 1971, 1200Z to 11, 0000Z
(c) February 12, 1971, 0000Z to 15, 1200Z
(d) March 19, 1971, 0000Z to 22, 1200Z

Data of three time periods are selected for this kinematic vertical motion study. These include time 4, the time of the southernmost penetration of cold air in terms of the 1000-500 mb thickness field, and 12 hours before and after (i. e. time 3 and time 5).

Undoubtedly, the compositing process will reduce the gradients of different variables somewhat since the cases chosen are only analogues, not identities. However, it is reasonable to expect that the smaller-scale features embedded in synoptic-scale systems will be largely filtered out. In addition, it is hoped that in the composite case most of the spurious random errors due to observation or processing will be eliminated. Furthermore, the diurnal variation is believed to be suppressed mostly in this composite case by choosing cases both at 0000Z and 1200Z. The significance of a composite case study lies in its greater representativeness as compared to the classical individual synoptic case study. Therefore, the compositing will help to insure that the results be more representative and the conclusions, hopefully, more significant.

(b) Data analysis

Mandatory (every 50 mb) and significant level radiosonde data were obtained for 94 station for each time period in each case covering the area bounded by 40°W to 120°W and 5°N to 50°N. The data source was the Northern Hemisphere Data Tabulation (NHDT) supplemented by Surface Synoptic and Marine Observations obtained from the National Climatic Center (NCC).

The few upper air observations not routinely available from the NHDT as well as those stations reporting only mandatory levels were obtained in their entirety from the NCC. Otherwise, missing data are linearly interpolated both in space and time. There were 15 stations with data available for only three of the four cases due to errors at the original source or the establishment or closing down of a station during the time period of this study. All data were then composited and processed for isobaric analysis.

Satellite and radar data were used to supplement the conventional data sources in the case selection and in checking the kinematically computed vertical velocity. Average surface elevation were obtained over one degree latitude-longitude quadrangles from the high resolution global terrain tape available from the National Center for Atmospheric Research (NCAR). The

topography is then smoothed by taking a 3 degree latitude by 3 degree longitude arithmetic mean centered at grid points.

Subjective analyses of isobaric surfaces were generated at 50 mb intervals with the aid of numerous vertical cross sections. Grid point data were then interpolated from the final analyses.

(c) Synoptic discussion of composite case

The general features of the synoptic situation are shown in Fig. 1 throngh Fig. 3.

At time 1 (not shown), the polar anticyclone was located over Montana with a 243 meter height at its center at 1000 mb. Weakening slowly at about a 10m $(12h)^{-1}$ rate, it moved rapidly southeastward across Wyoming and Colorado into Texas at time 3. The surface center, under the northwesterly flow aloft, moved farther southeastward into the Gulf of Mexico at time 4 then turned eastward and eventually northeastward (see Fig. 1). The cyclone of interest in this study developed on a trailing polar front which was located over the Southern States at time 1 and 2. Cyclogenesis took place at time 3 over Georgia (see Fig. 1A). This cyclone then moved northeastward to North Carolina at time 4 (see Fig. 1B) and to a position east of the New Jersery coast at time 5 (see Fig. 1C) with a 60m $(12h)^{-1}$ surface height fall at its center. While continuing to move northeastward after time 5, it showed no further deepening for the rest of time periods.

At 850 mb, the major trough in the westerlies was located over the Great Plains and extended southwestward into Mexico at time 1. While this trough intensified slightly and moved eastward into the southern States and the Gulf of Mexico, a closed circulation formed over the Great Lakes at time 2 (not shown). The trough moved slowly southeastward and intensified

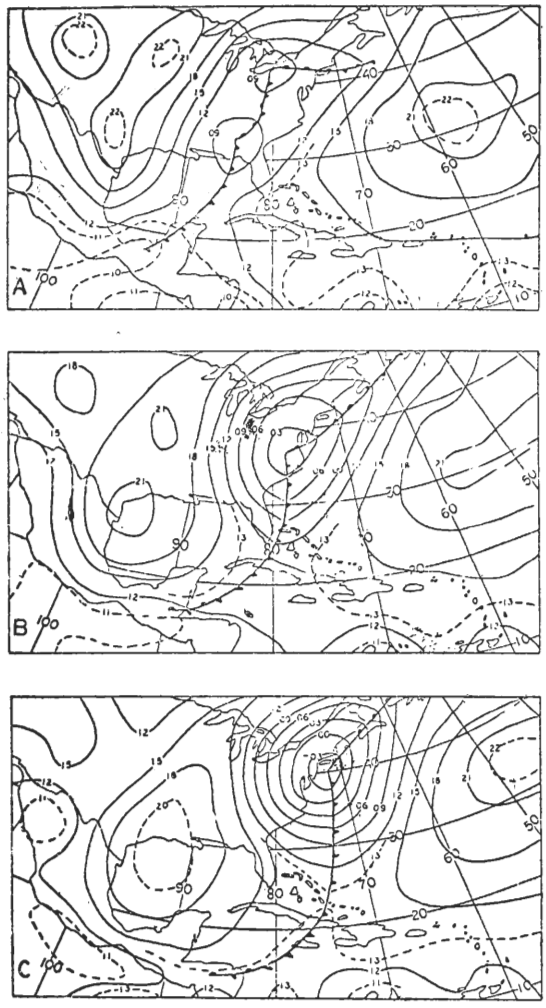

Fig. 1. Surface map (1000 mb) at time 3 (A), time 4 (B), and time 5 (C). Contour lines are drawn every 3 dam; dashed every 1 dam where necessary

rapidly from time 2 to time 3 concomitant with the surface cyclogenesis. It then accelerated eastward and intensified further until time 5, and then weakened during the remaining time periods. The intensification and weakening of the trough can be detected in the vorticity field. The closed low, while moving eastward slowly, deepened until time 6, after which it filled. The high-pressure center originally located over Montana at time 1 moved rapidly southeastward into the Texas-Mexico area at time 3.

This high center then moved slowly southeastward into the Gulf of Mexico until time 5 and then slowly eastward during the remaining time periods. Note that the high centers at 850 mb were located to the west or southwest of the corresponding surface centers (see Fig. 1, 2). The former is hydrostatically consistent with warmer air being located to the southwest of the high center in the lower layer where warm advection prevails.

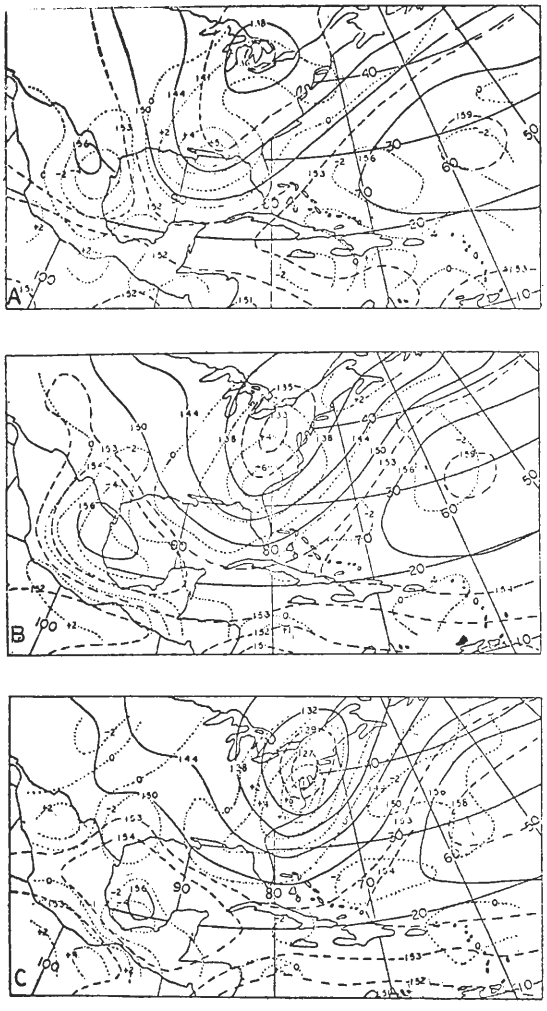

Fig. 2. 850 mb map at time 3 (A), time 4 (B), and time 5 (C). Contour lines (solid) are drawn every 6 dam;dashed every 3 (or 1) dam where necessary. Dotted lines are relative vorticity at 2×10^{-5} sec^{-1} intervals; at 1×10^{-5} sec^{-1} intervals where necessary.

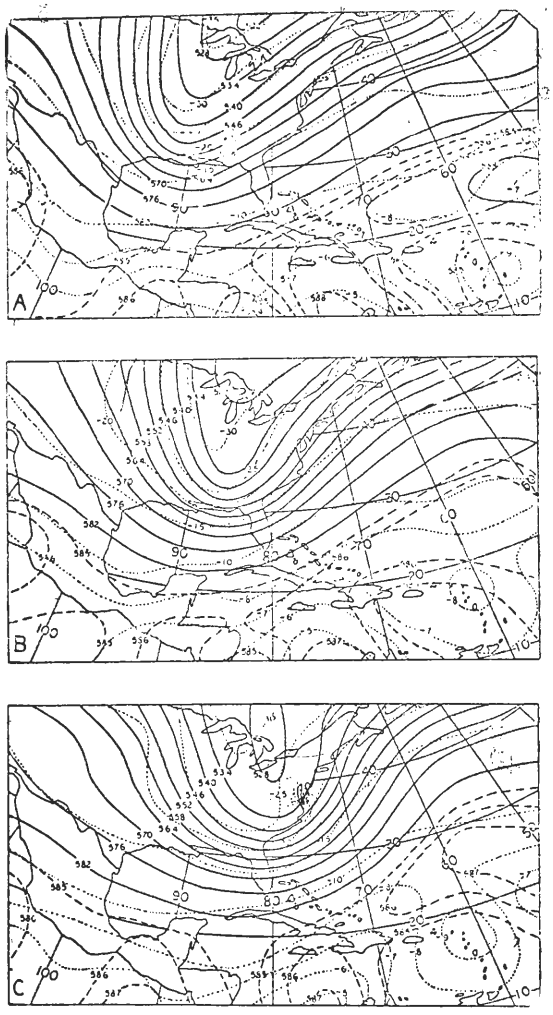

Fig. 3. 500 mb map at time 3 (A), time 4 (B), and time 5 (C). Contour lines are drawn every 6 dam; dashed every 3 (or 1) dam where necessary. Dotted lines are isotherms at 5°C intervals; at 2°C (or 1°C) inervals where necessary.

At 500 mb the main trough was located to the lee of the Rockies at time 1 (not shown) and the thermal trough layed further upstream, suggesting intensification. The trough moved eastward at 15 m s^{-1} intensified further as the thermal trough continued to lag, and was situated over the Great Plains and the Gulf of Mexico at time 3. This trough moved at a nearly constant speed eastward for the rest of the

time periods and weakened after time 5, as suggested by the thermal field. The intensification and weakening of the trough can also be easily detected in the vorticity field (not shown). A northerly component of the flow over the Gulf of Mexico is believed to be instrumental for the deep penetration of cold air into low latitudes.

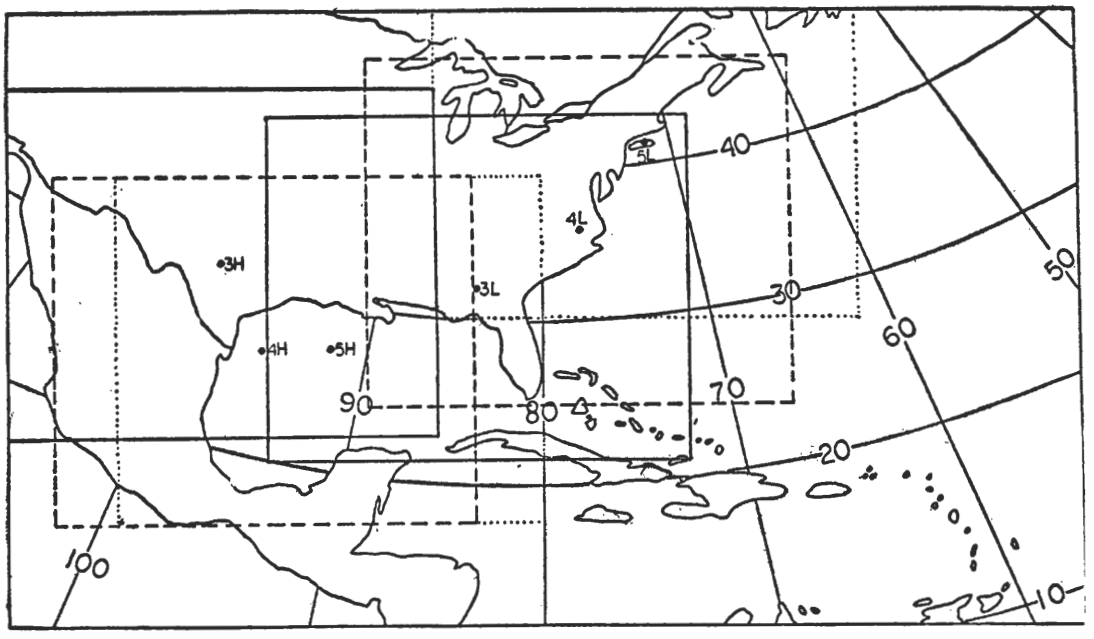

Fig. 4. Limited region moving with the surface anticyclone (H) and cyclone (L). Solid, dashed, and dotted lines are boundaries at times 3, 4, and 5, respectively.

3. Computational Procedures

Symbols used in the equations are listed as follows:

C_d	skin drag coefficient
C_{gs}	geostrophic drag coefficient
C_p	specific heat at constant pressure
$\bar{D}$	averaged horizontal divergence in the layer
D'	adjusted horizontal divergence
f	Coriolis parameter
g	gravitational acceleration
h	surface topography
ΔP	Pressure increment
R	gas constant for dry air
R_{os}	surface Rossby number
T	temperature
T_s	temperature at surface
$\bar{u}$	X component of wind averaged in the layer
u_s, u_{gs}	X component of thc surface wind and geostrophic wind
$\vec{V}, V$	wind vector and wind speed
$\vec{V}_s, V_s$	wind vector and wind speed at surface
$\bar{v}$	Y component of wind averaged in the layer
v_s, v_{gs}	Y component of the surface wind and geostrophic wind
V_{gs}	surface geostrophic wind speed
w	vertical wind speed in (X,Y,Z)
ω	vertical wind speed in (X,Y,P)
ω'	adjusted vertical wind speed
ω_o	vertical velocity at surface
ω_K	vertical velocity at upper boundary computed from kinematic method

ω_T vertical velocity at upper boundary computed from adiabatic method

ω_t orographic induced vertical velocity at lower boundary

ω_f frictional induced vertical velocity at lower boundary

z height

z_o aerodynamic roughness parameter

α_o angle formed by surface stress and geostrophic wind

ρ_s air density at surface

θ wind direction

The kinematic method for computing the vertical velocity has its primary advantage in mathematical simplicity, hydrostatic balance being its only physical assumption. Previous studies (Lateef 1967, Fankhauser 1969, Smith 1971, Schmidt and Johnson 1972) indicated that the reliability of the kinematic method is sufficient for use in diagnostic studies if some techniques are employed to reduce the cumultive observational and computational errors. Thus, the special adjustment criteria developed by O'Brien (1970) were employed in the horizontal divergence and vertical velocity computations in this study.

The mean divergence $\bar{D}$ of the horizontal wind for arbitrary pressure layer can be computed from the following equation

$$\bar{D}_k=\left(\frac{\partial \bar{u}}{\partial x}\right)_k+\left(\frac{\partial \bar{v}}{\partial y}\right)_k \qquad (1)$$

where $\bar{u}$ and $\bar{v}$ represent averaged velocity components in the layer k.

Integration of the continuity equation,

$$\frac{\partial \omega}{\partial p}+\bar{D}_k=0 \qquad (2)$$

yields the vertical velocity at the top of all layers k as:

$$\omega_k=\omega_{k-1}+\bar{D}_k\ \Delta P\ (\Delta P=50\text{mb}) \qquad (3a)$$

or

$$\omega_k=\omega_o+\sum_{i=1}^{k} D_i\ \Delta P \qquad (3b)$$

where ω_o is the vertical velocity at the lower boundary.

The adjusted divergence D′ and vertical velocity ω' can be written as:

$$D_k'=\bar{D}_k-\frac{k}{M}(\omega_K-\omega_T)\ /\Delta P \qquad (4)$$

$$\omega_k'=\omega_k-(\omega_K-\omega_T)\frac{k}{2M}\ (k+1) \qquad (5)$$

$$\text{where}\quad M=\sum_{k=1}^{N} k=\frac{1}{2}\ N\ (N+1) \qquad (6)$$

and N is the total number of layers.

In equation (4) and (5), ω_K is the unadjusted vertical velocity at upper boundary as obtained from (3a) or (3b), and ω_T is the specified boundary value at the same level. In this study, the ω_T values are computed by the adiabatic method, a technique successfully used by Lateef (1968) in computing the vertical velocity at 100 mb. The correction term in (4) and (5) is a linear function of pressure. It is reasonable since the wind measurements tend to deteriorate with increasing height. Large corrections, thus, occur in the upper levels but only small corrections in the lower levels. This adjustment technique was proved to be more realistic than the others by correlating the ω values to the observed cloudiness, precipitation and radar echoes (Smith, 1971).

The vertical velocity at the upper boundary ω_T is computed by using the adiabatic method where

$$\omega_T=\left(\frac{\partial T}{\partial t}+\vec{V}\cdot\nabla T\right)\Big/\left(\frac{RT}{C_pP}-\frac{\partial T}{\partial P}\right) \qquad (12)$$

At the lower boundary ω arises from two causes: (1) an orographic vertical motion ω_t due to flow along a sloping terrain; (2) a frictional vertical motion ω_f due to divergence or convergence within the surface boundary layer. The surface

boundary layer is taken to be the lowest 1 km (or lowest 100 mb) (Sutton 1953, Priestly 1959, and Munn 1966).

Results of an observational study by Lilly (1971) suggest that the synoptic-scale induced vertical velocity ω_t vanishes at about 500 mb level. It, therefore, seems reasonable to linearly interpolate ω_t to 900 mb from its surface value. Values of ω_o at the lower boundary, thus, can be computed as follows: (Sawyer 1959, Cressman 1960, Krishnamurti 1968a)

$$\omega_t = -\rho_s g w_o = -\rho_s g \vec{V}_s \cdot \nabla h \qquad (8a)$$

$$\omega_f = \frac{g}{f}\left[\frac{\partial}{\partial y}(C_d \rho_s u_s \sqrt{u_s^2+v_s^2}) - \frac{\partial}{\partial x}(C_d \rho_s v_s \sqrt{u_s^2+v_s^2})\right] \qquad (8b)$$

$$\omega_o = \omega_t + \omega_f \qquad (8c)$$

Here, h is the topography and all the other variables refer to the surface (1000 mb) values. As Kung (1963) noted, Cressman's (1960) C_d values are overestimates over mountain areas. Therefore, the geostrophic drag coefficient C_{gs} computed from Lettau's model (1959, 1961) and surface geostrophic wind have also been used for computing ω_f in (8b).

Since the wind observations below 850 mb are not available over most of the stations with high elevations, the 1000 mb wind is, therefore, computed by using the logrithmic wind profile and Lettau's model as follows:

$$R_{os} = V_{gs}/z_o\, f \qquad (9a)$$

$$C_{gs} = 0.205/(\log_{10} R_{os} - 0.566) \qquad (9b)$$

$$V_s = 2.5\, C_{gs}\, V_{gs} \ln\left(\frac{z}{z_o}\right) \qquad (9c)$$

$$\theta = \tan^{-1}\left(\frac{v_{gs}}{u_{gs}}\right) \qquad (9d)$$

$$u_s = V_s \cos(\theta+\alpha_o) \qquad (9e)$$

$$v_s = V_s \sin(\theta+\alpha_o) \qquad (9f)$$

Where Z=10 meters The wind at 900 mb is, therefore, linearly interpolated between 1000 mb and 850 mb.

One of the results from Kung's (1963) study of conditions of the boundary layer is that the vegetative cover, rather than topography, represent the most efficient roughness structure over land areas. Therefore, the aerodynamic roughness parameter Z_o was taken from Kung's (1965) winter estimates, over the continents, and was prescribed over the oceans and the islands (over the ocean Z_o=0.1 cm; over the tropical islands Z_o=5 cm; over the mid-latitude islands Z_o=1 cm). (Kung 1963, Munn 1966).

A computational domain of 13 by 13 was employed for both the cyclone and anticyclone with a grid spacing of 254 km valid at 60°N on a polar stereographic map. Essentially, the computational domain encompasses the entire region within the outermost closed surface isobar of the composite cyclone and anticyclone.

As mentioned in the previous section, the data used in this study are interpolated from a subjective analysis. A two-dimensional filter is, therefore, necessary to eliminate short-wavelength components from the final analysis. A 25-point filter, originally designed by Bleck (1965) and succssfully used by Bosart (1970), is adopted for this purpose at the inner points of the limited region. The gradients and absolute magnitude of the various meteorological parameters in the initial analyses were well preserved by this filter. A 9-point filter, used by Shuman (1957), is applied at the outer and inner boundary points with ν=0.5 in his equation (5). These two filters have proved the most successful at filtering out the short-wave noise, while retaining the large scale features (loc. cit.).

4. Results of Computation

(a) Surface Anticyclone

Patterns of adjusted vertical velocity (ω', dashed) at different levels and different times for the surface anticyclone are shown in Fig. 5a through 5c.

At 850 mb, downward motion was found in the eastern sector where north-north-westerly flow prevailed and upward motion in the western sector where a southeasterly return flow dominated. At time 3, an area of maximum downward motion was located to the southeast of the surface center where cold advection prevailed. Upward motion was observed in the vicinity of the surface center to the west and southwest perhaps mostly due to orographic lifting. The eastern half of the area was occupied by weakening downward motion and the western half by intensifying upward motion at time 4. At time 5, the overall magnitude decreased and downward motion dominated most of the eastern sector and spread over part of the western sector whereas upward motion was confined to the farther western area. An area of maximum gradient was found to the southeast of the surface center at time 3, it moved to the south and intensified at time 4 and then moved to the southwest and weakened at time 5.

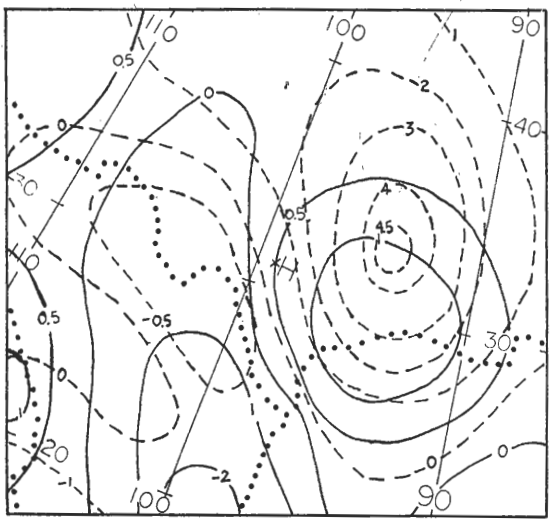

Fig. 5 (a). Vertical velocities over the surface anticyclone at time 3 for 850 mb (solid) and 500 mb (dashed). Isoplethes are drawn at 1 μb sec^{-1} intervals and at 0.5 μb sec^{-1} intervals where necessary. Dotted lines indicate the geography.

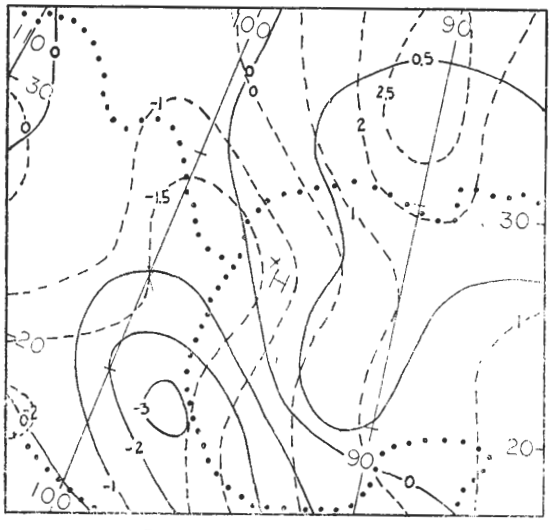

Fig. 5 (b). Same as Fig. 5(a), except at time 4.

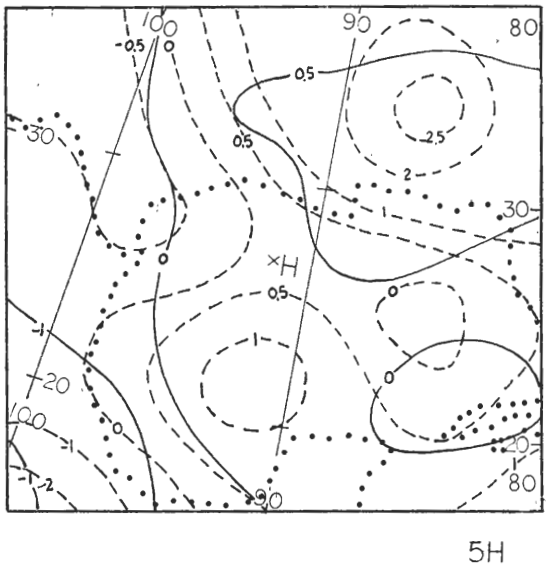

Fig. 5 (c). Same as Fig. 5(a), except at time 5.

At 500 mb, a well organized downward motion pattern was found in the eastern sector at time 3 with a maximum value of 4.5 μb s^{-1} to the east-north-east of the

surface center. Weak upward motion was still present in the western sector. The downward motion weakened and still occupied the eastern sector with an area of maximum value moving to the northeast of the surface center at time 4. Upward motion in the western sector intensified somewhat primarily due to the favorable condition for orographic upslope motion in the lower boundary. At time 5, downward motion dominated the eastern sector and spread over part of the western sector with areas of maximum values to the northeast and the south of the surface center; whereas upward motion was confined to the far western part of the area. An area of maximum gradient was located to the east of the surface center at time 3, it moved to the northeast at time 4 and then moved to the northwest at time 5.

The overall pattern of the vertical motion appears to be synoptically reasonable at 200 mb although the absolute magnitude is questionable in view of the relatively large adjustment at this level (not shown). Comparing the patterns of vertical velocity at 850, 500, and 200 mb, we find that the maximum downward motion was reached at 500 mb, to the northeast of the surface center while the maximum upward motion was located at 850 mb to the southwest. The patterns are vertically consistent in spite of a small vertical shift of the maximum centers northward. The details of the vertical structure will be discussed next.

The vertical cross sections of the vertical velocity from southwest, passing through the center of the surface anticyclone, to northeast, are shown in Fig. 6. In general, downward motion prevailed over the northeastern section and upward motion over the southwestern section, at all levels. At time 3 Fig. 6(a), downward motion was found over the northeastern half at all levels with a maximum value of 3.8 μb s^{-1} at 450 mb. There was a small region of downward motion to the extreme southwest

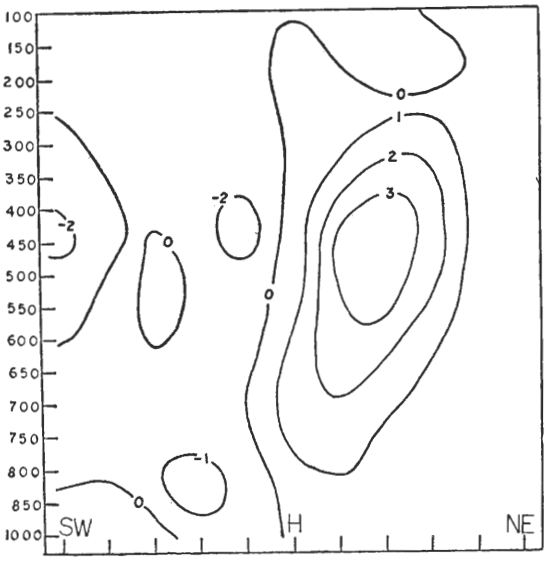

Fig. 6 (a). Vertical cross sections of the vertical velocity for the surface anticyclone from southwest (to the left of figure), passing through surface center, to northeast (to the right of figure) at time 3. Vertical axis shows the pressure level in mb. Isoplethes are drawn at 1 μb sec^{-1} intervals

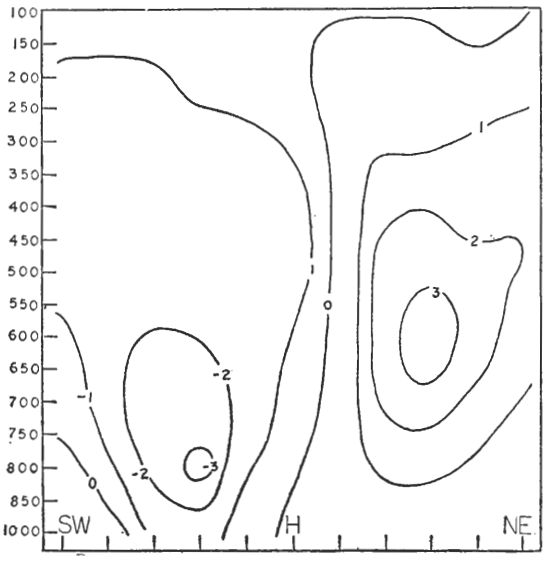

Fig. 6 (b). Same as Fig. 6(a), except at time 4.

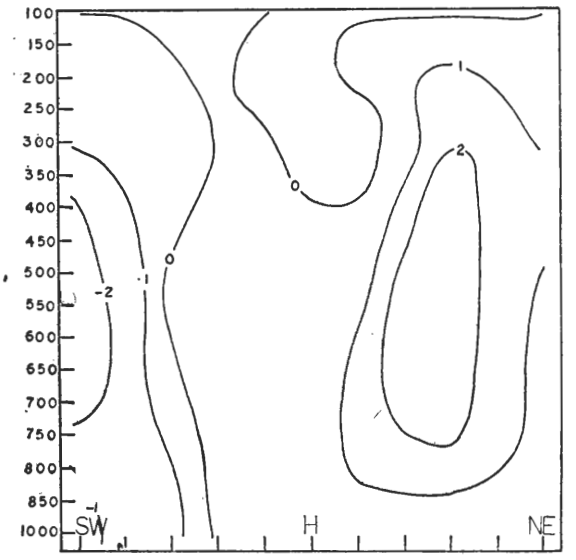

Fig. 6 (c). Same as Fig. 6 (a), except at time 5.

of the lower troposphere due to the downslope motion west of the Mexican mountain with a maximum value of 1.2 μb s^{-1} at 1000 mb and another small area of weak downward motion in the midtroposphere to the southwest of the surface center. Upward motion was observed in most of the southwestern section with a maximum value of -2.0 μb s^{-1} at 450 mb to the extreme southwest and secondary maxima of -1.3 μb s^{-1} at 850 mb and -1.2 μb s^{-1} at 450 mb to the near southwest. A dipolar pattern was well-developed at time 4 with a maximum downward motion of 3.4 μb s^{-1} at 600 mb to the northeast of the surface center and a maximum upward motion of -3.0 μb s^{-1} at 800 mb to the southwest. Small values of upward motion over the center of the surface anticyclone are presumably due to the boundary orographic upslope motion which decreased upward gradually. A small area of downward motion to the farther southwest of the surface center in the lower troposphere was still discernible. At time 5, downward motion dominated the northeastern part and spread over the southwestern part of the troposphere. Upward motion was mainly found in the far southwestern section at all levels and in a small region over the surface center in the upper troposphere. Maximum downward motion reached a value of 2.7 μb s^{-1} located at 550 mb to the northeast of the surface center while maximum upward motion of -2.9 μb s^{-1} occurred at the same level to the southwest. Note that the center of maximum downward motion moved northeastward and downard with its intensity weakened from time 3 to time 5 while the surface anticyclone moved southeastward.

(b) Surface Cyclone

Figs. 7 (a) through 7 (c) show the adjusted vertical velocity of the surface cyclone at different levels and different times.

At 850 mb, weak upward motion occupied most of the area of interest at time 3 except to the west of the surface center where downward motion was observed. The upward motion increased in intensity

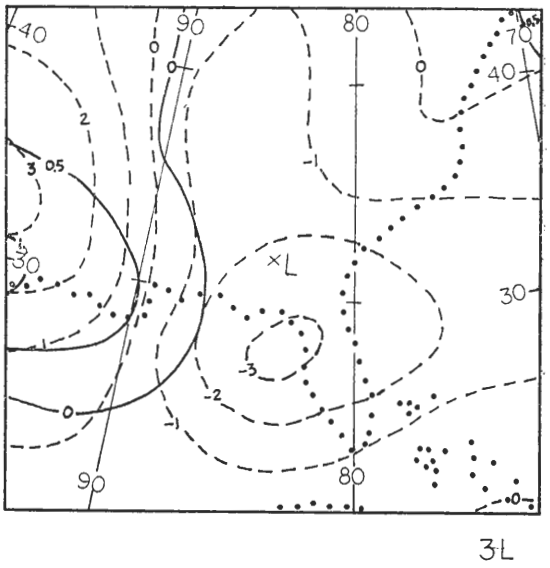

Fig. 7 (a). Same as Fig. 5 (a), except at time 3 over the surface cyclone.

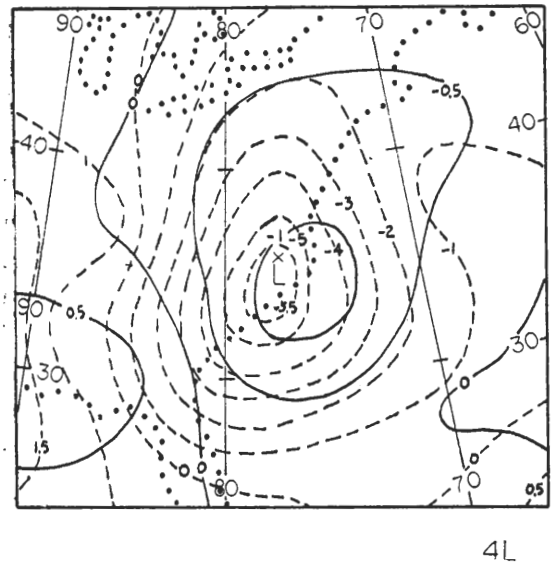

Fig. 7 (b). Same as Fig. 7 (a), except at time 4.

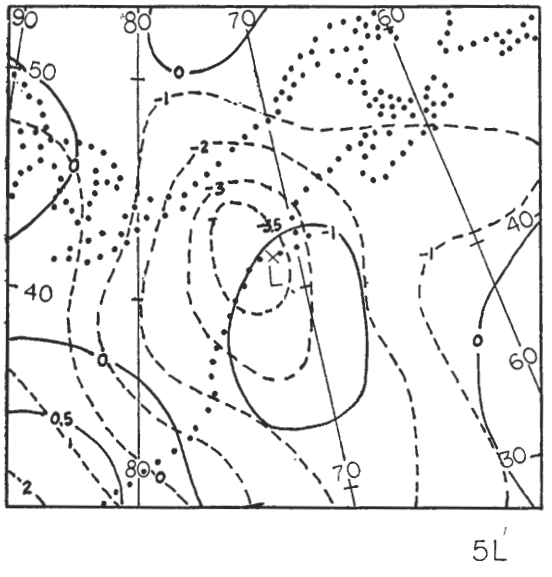

Fig. 7 (c). Same as Fig. 7 (a), except at time 5.

and still occupied most of the area at time 4, except for a small region to the southeast of the surface center and the extreme western sector where downward motion was found, An area of relatively strong upward motion developed over the surface center with a maximum value of $-1.1\ \mu b\ s^{-1}$ to the immediate south. At time 5, the upward motion further intensified and spread over most of the area of interest. A center of maximum upward motion was found to the south of the surface center with a value of $-1.4\ \mu b\ sec^{-1}$. An area of maximum gradient was found to the west of the surface canter at time 3, it moved to the southwest and intensified at time 4 and then weakened at time 5.

At 500 mb, most of the area was occupied by upward motion at time 3 except for some areas farther away from the surface center. Strong upward motion was over the surface center with a maximum value of $-3.0\ \mu b\ sec^{-1}$ to the south. Strong upward motion was well-developed over the surface center at time 4, with a maximum value of $-5.8\ \mu b\ sec^{-1}$ to the near south with weakening downward motion to the far western sector of the surface center. Upward motion decreased in intensity overall at time 5 but occupied a larger area than at times 3 and 4. Downward motion was confined to a small area southwest of the surface center. The maximum upward motion decreased to a value of $-3.9\ \mu b\ s^{-1}$ right over the surface center.

Comparing the vertical velocity patterns at 850, 500, and 200 mb (not shown), we find that both upward and downward motion reached maximum intensity at 500 mb. Upward motion was the rule at all levels in the troposphere over the cyclone area, except for a region to the southwest of the surface center where downward motion was present. The details of the vertical structure of the vertical velocity patterns will be discussed next.

The vertical cross sections of the vertical velocity field from northwest, passing through the center of the surface cyclone, to southeast, are shown in Fig. 8. At time 3, most of the area was occupied

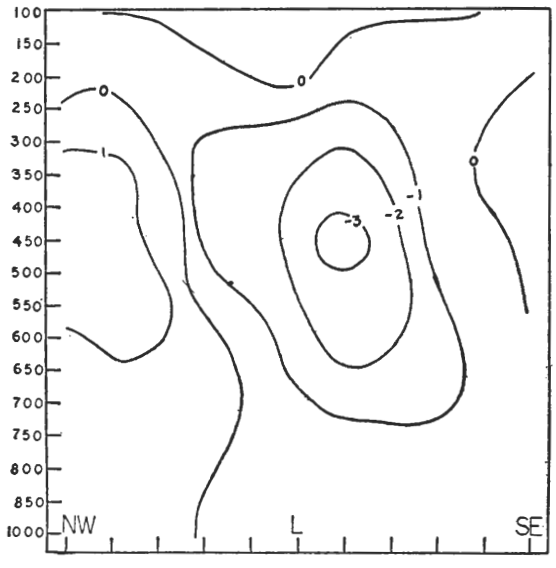

Fig. 8 (a). Same as Fig. 6 (a), except for the surface cyclone from northwest (to the left of figure), passing through surface center, to southeast (to the right of figure) at time 3.

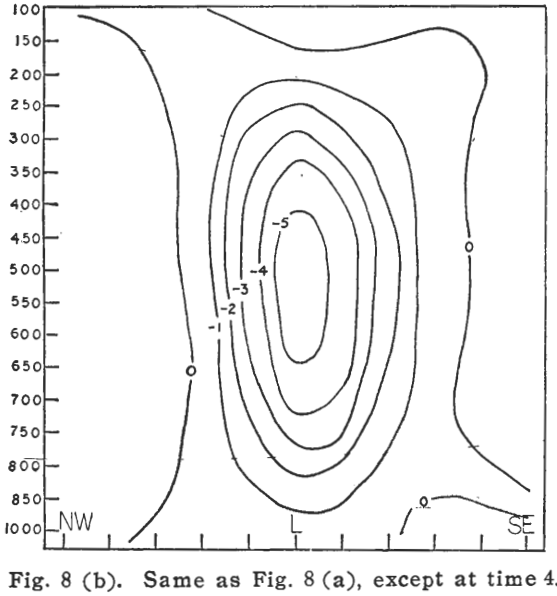

Fig. 8 (b). Same as Fig. 8 (a), except at time 4.

by upward motion in the vicinity of the surface center. Downward motion was observed mainly to the northwest of the surface center in the mid- and lower troposphere. An area of strong upward motion was found to the immediate southeast of the surface center with a maximum value

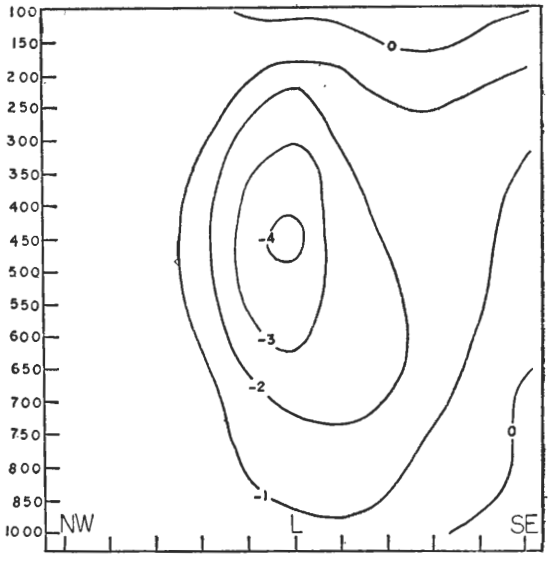

Fig. 8 (c). Same as Fig. 8 (a), except at time 5.

of -3.1 μb sec^{-1} at 450 mb. At the same level, a maximum downward motion of 1.9 μb sec^{-1} was also observed to the northwest of the surface center. At time 4, upward motion intensified and became better-organized at all levels in the vicinity of the surface center. Weak downward motion was present to the far southeast and northwest of the surface center at all levels. The maximum upward motion reached a value of -5.6 μb sec^{-1} at 500 mb. At time 5, upward motion decreased in intensity but dominated more area than at times 3 and 4. Maximum upward motion was now located right over the surface center as would be expected for an occluding cyclone and decreased to a value of -4.1 μb s^{-1} at 450 mb In general, cross sections show that upward motion was the rule over the surface cyclone at all levels with a maximum intensity reached at about the 500 mb level; downward motion was confined to the rather limited region to the far southeast and northwest of the surface center.

(c) Average vertical profiles

The adjusted vertical velocity ω' is shown in Figs. 9 and 10 averaged over the entired area of 3×3 grid points centered

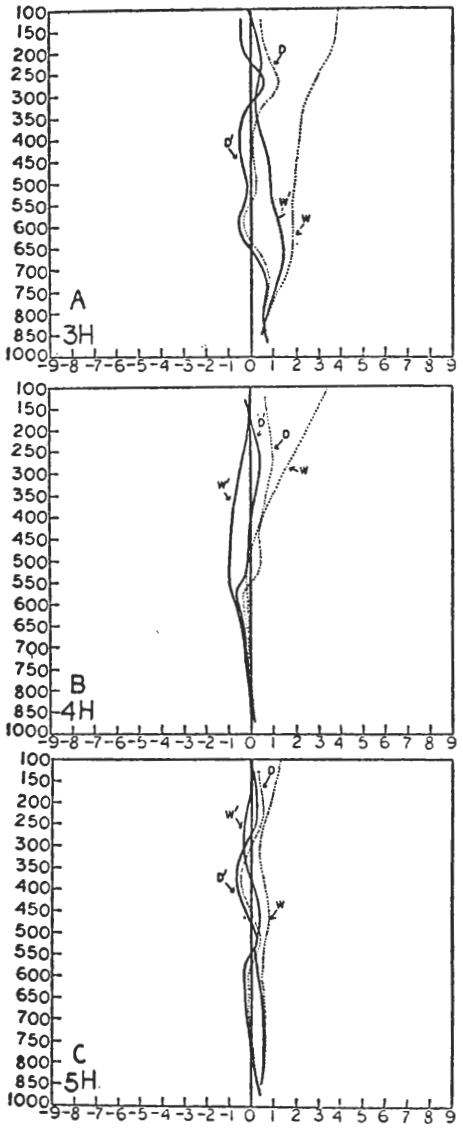

Fig. 9. Vertical profiles of averaged values of divergence D in 10^{-5} sec^{-1} and vertical velocity ω in μb sec^{-1} over 3×3 grid centered at surface anticyclone for time 3 (A), time 4 (B), and time 5 (C). The profiles of D′ and ω' refer to the adjusted values, while D and ω refer to the values obtained from the observational wind field.

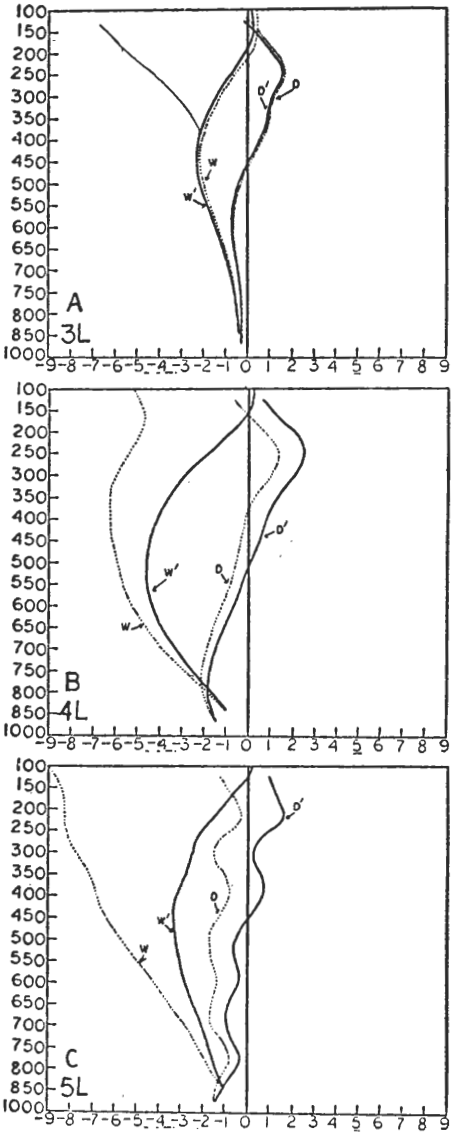

Fig. 10. Same as Fig. 9 except for surface cyclone at time 3 (A), time 4 (B), and time 5 (C).

on the surface anticyclones and cyclones. Over the central region of the surface anticyclone, downward motion was found at time 3 at all levels with a maximum value located around 700 mb. Upward motion was observed at time 4 at all levels with a maximum value located around 500 mb. The averaged upward motion in the vicinity of the surface center is due to the lower boundary condition which is very favorable

for orographic upslope motion in the western section of the surface anticyclone at this time. However, downward motion was found when averaged over larger area (e.g. 7×7 and 11×11 grids). At time 5, downward motion was observed in the lower and mid-troposphere and upward motion in the upper troposphere. Over the central region of the surface cyclone, upward motion prevailed at all levels except in the upper troposphere where slight downward motion was observed. The maximum intensity of upward motion was found around 500 mb at all times.

5. Discussions

Radar reports on clouds for four cases received from NWS over the facsimile were composited using data from 1145 GMT and 2345 GMT for time 1200 GMT and 0000 GMT, respectively. These are presented in Fig. 11 using the NWS conventional symbols. Comparing the distributions of clouds and echo tops with the vertical motion fields

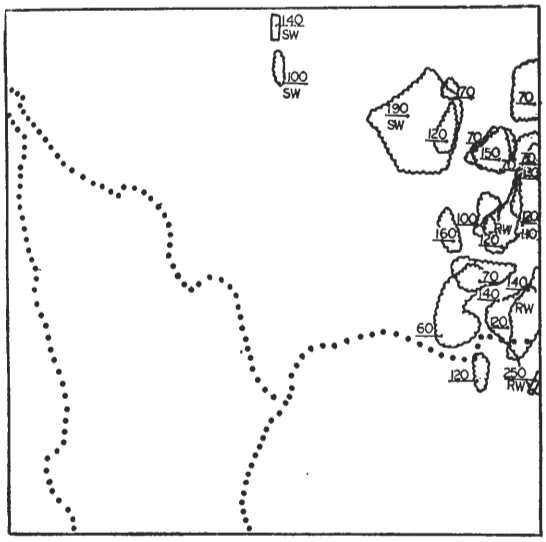

3H

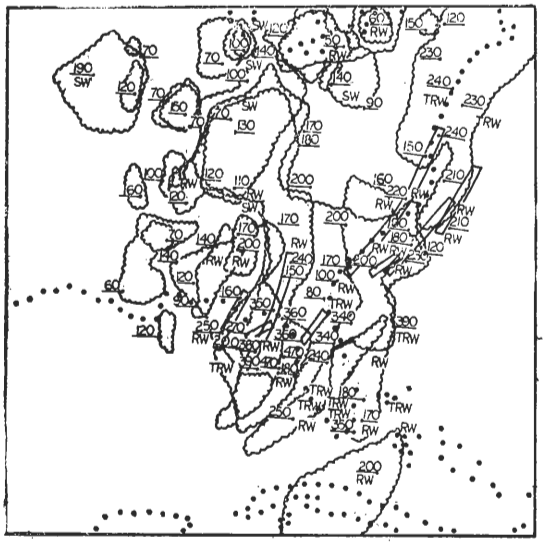

3L

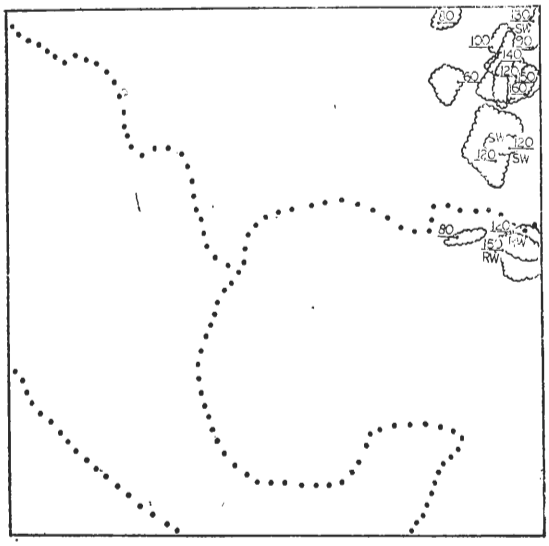

4H

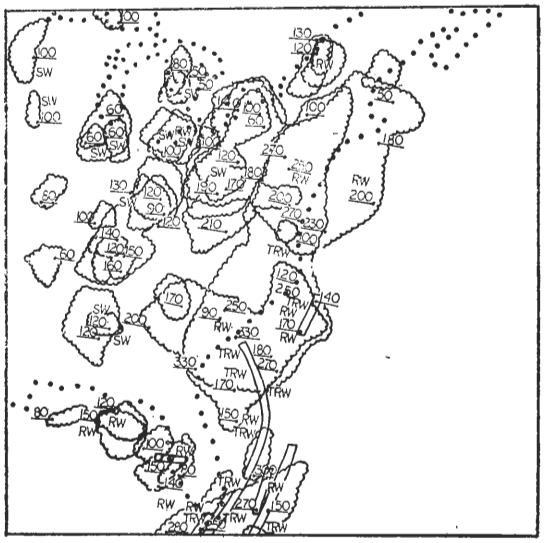

4L

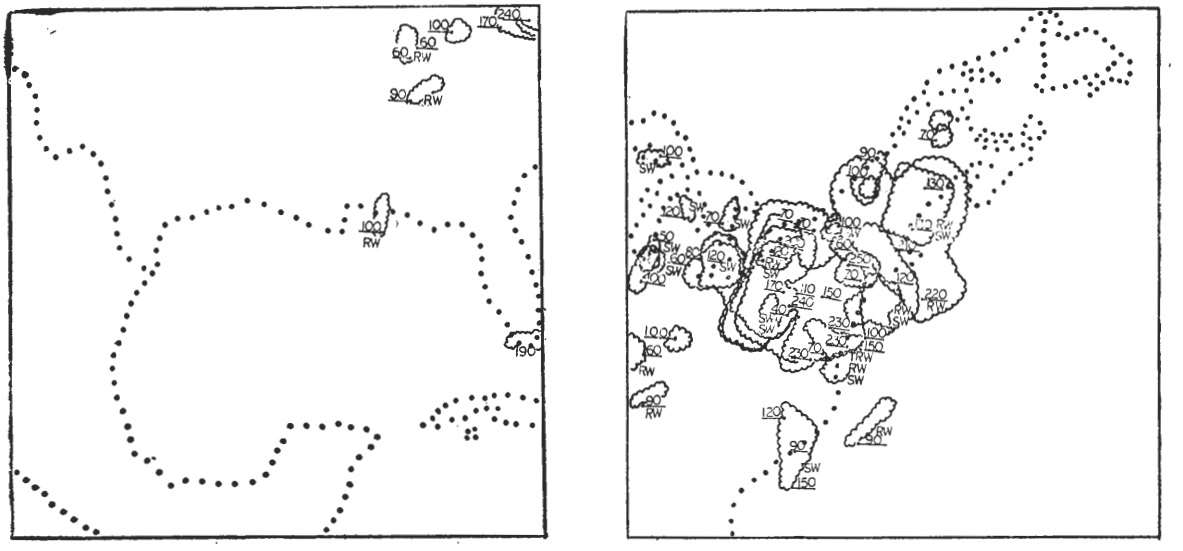

Fig. .11 Composite radar reports from time. 3 to time 5 for anticyclone (H) and cyclone (L). Numerical values indicate the heights of echo tops in hundreds of feet. Symbols are NWS conventional. Dotted line indicates geography.

presented earlier, we find that the cloud tops were mostly confined in the lower troposphere over the eastern region of the surface anticyclone where downward motions at all levels were observed. Over the surface cyolone, on the other hand, the clouds with higher tops were found over the region where upward motions at all levels were observed; while the clouds with lower tops were found over the region where downward motion at 200 mb prevailed. The strongest upward motion at 500 mb was found over the area where the highest tops of the clouds were also observed. This is synoptically consistent as far as the large scale motion is concerned. The adjusted vertical motion fields, therefore, seem to be reasonable in view of the radar cloud observation.

Comparisons of maximum vertical motion computed by different techniques are presented in Table 1. While different synoptic cases used can at least partially account for the different values, the overall magnitudes are certainly comparable. Note also that a composite case was analyzed in the present study while the individual cases were used for the other investigations.

In contrast to the other investigations, the maximum centers were found to the northeast of the surface highs and to the near south of surface lows in the present study. This is believed to be due to the present case selection of deep polar air outbreaks into low latitudes with the axis of high and low centers approximately along a NE-SW direction in contrast to the general E-W Orientation in the other case studies.

In spite of the finer details, the magnitude and patterns of the vertical velocity of this study are comparable to results of previous studies in which the kinematic method (Murakami 1958, Palmen and Holopainen 1962, and Smith 1971), the quasi-geostrophic ω equation (Sanders et al 1960, Cressman 1961, Sanders 1963, Danard 1964, and Haltiner et al 1965), or the balanced ω

Table 1. Examples of maximum vertical velocity (ω) at 500 mb using different computational techniques. ω_s: special adjustment technique used in the present study; ω_Q: quasi-geostrophic ω-equation; ω_B: balance ω-equation.

Author	Data	(μb s^{-1})	Remarks
Smith (1971)	March 21, 1962, 1200Z	6.7 (ω_S)	S of surface high
		-6.5 (ω_S)	ENE of surface low
Krishnamurti (1968b)	April 13, 1964, 1200Z	8 (ω_Q)	E of surface high
		-7 (ω_Q)	N of surface low
		4 (ω_B)	E of surface high
		-6 (ω_B)	N of suraface low
Present study			
	3H	4.5 (ω_S)	ENE of surface high
	4H	2.8 (ω_S)	NE of surface high
	5H	2.7 (ω_S)	NE of surface high
	3L	-3.0 (ω_S)	near S of surface low
	4L	-5.8 (ω_S)	near S of surface low
	5L	-3.9 (ω_S)	right over surface low

equation (Krishnamurti 1968b) were used for synoptic-scale systems in the extratropics.

6. Conclusions

The main objective of this paper is to analyze the distribution of kinematic vertical motions, using O'Brien's (1970) adjustment technique, for a composite case of winter time polar air outbreaks penetration into lower latitudes. It was found that the downward motion prevailed over the area of surface anticyclone with its maximum intensity located in the vicinity of 550 mb to the northeast of surface center. Maximum values reached 4.5 μb s^{-1}, 2.8 μb s^{-1}, and 2.7 μb s^{-1} at time 3, 4, and 5, respectively. Upward motions prevailed in the vicinity of the surface cyclone with the maximum intensity usually located at 450 mb level to the near south of the surface center. Maximum values reached -3.0 μb s^{-1}, -5.8 μb s^{-1}, and -3.9 μb s^{-1} at time 3, 4, and 5, respectively. The magnitudes and general patterns are comparable to the results obtained in previous case studies (loc. cit.). Radar reports indicated that the computed kinematic ω's are in reasonably good agreement with the cloud echoes.

Acknowledgment

The author would like to exprese his great appreciation to Professors Griffith Wang and Ching-Yen Tsay for discussions and valuable suggestions. Thanks are to Mr. Ching-Chi Wu for drawing some of the diagrams.

References

Bleck, R., 1965: Lineare Approximations methoden zur Bestimmung ein-und zweidimensionaler numerischer filter des dynamischen meteorologie. Institut fur Theoretische Meteorologie der Freien. Universitat Beilin.

Bosart, L. F., 1970: Mid-tropospheric frontogenesis. *Quart. J. Roy. Meteor. Soc.*, 96, 442-471.

Bullock, B. R., L. H. Horn and D. R. Johnson (1969): The contribution of infrared cooling to the vertical motion field and its implication in atmospheric energenetics. *Mon. Wea. Rev.*, 97. 371-381.

Cressman, G. P., 1960: Improved terrain effects in barotropic forecasts. *Mon. Wea. Rev.*, 88, 327 -344.

Cressman, G. P., 1961: A diagnostic study of mid-tropospheric development. *Mon. Wea Rev.*, 89, 74-82.

Danard, M. B., 1964: On the influence of released latent heat on cyclone development. *J. Appl Meteor.* 3, 27-37.

Danielsen, E F., 1961: Trajectories: Isobaric, isentropic and actual. *J. Meteor.*, 18, 479-486.

Fankhauser, J. C., 1969: Convective processes resolved by a mesoscale rawinsonde network. *J. Appl. Meteor.*, 8, 778-798.

Haltiner, G. J., and R. F. Alden, and G. C. Rosenberger, 1965: On the structure of pressure systems. *Mon. Wea. Rev.*, 93, 297-305.

Krishnamurti, T. N., 1968 (a): A diagnostic balance model for studies of weather systems of low and high latitudes, Rossby number less than 1. *Mon. Wea. Rev.*, 96, 197-207.

Krishnamurti, T. N., 1968 (b): A study of a developing wave cyclone. *Mnn. Wea. Rev.*, 96, 208-217.

Kung, E., 1963: Climatology of aerodynamic roughness parameter and energy dissipation in the planetary boundary layer over the North Hemisphere. Annual Rep. Cont., DA-36 -039-AMC-00878, Dept. of Met., U of Wisc., 37-96.

Kung, E., 1965: Aerodynamic roughness of the earths surface: A parameterization for use in general circulation studies. (unpublished paper)

Lateef, M. A., 1967: Vertical motion, divergence, and vorticity in the troposphere over the Caribbean, August 3-5, 1963. *Mon., Wea. Rev.*, 95, 778-790.

Lateef, M. A., 1968: Vertical motion at 100 mb in the tropics *Mon. Wea. Rev.*, 96, 286-290

Lettau, H. H., 1959: Wind profile, surface stress and geostrophic drag coefficient in the atmospheric surface layer. *Advan. in Geophy.*, 6, 241-255

Lettau, H. H., 1961: Theoretical wind spiral in the boundary layer of a barotropic atmosphere. Ann. Rep. Cont. DA-36-039-80 282, Dept. of Met. U Wisc.

Lilly, D. K., 1971: Observation of mountain-induced turbulence. *J. Geophys. Res.*, 76, 6585-6588.

Munn, R. E., 1966: *Descriptwe micrometeorology.* Academic Press, 245 pp

Murakami, T., 1958: Numerical analysis of wind and its application to the numerical weather forecasting (part I). *J. Meteor. Soc. Japan*, 36, 11-22.

O′ Brien, J. J, 1970: Alternative solutions to the classical vertical velocity problem. *J. Appl. Meteor.*, 9, 197-203.

Palmén, E., and E. O. Holopainen, 1962: Divergence, vertical velocity and conversion between potential and kinetic energy in an extratropical disturbance. *Geophysica*, 8, 89-114.

Priestly, C. H. B., 1959: *Turbulent transfer in the lower atomsphere* The Univ. of Chicago Press.

Sanders, F., A. J Wagner and T. N. Carlson, 1960: Specification of cloudiness and precipitation by multi-level dynamical models. Dept. of Met., MIT, Sci. Rep., #1.

Sanders, F, 1963: Further research directed toward the study of relations of atmospheric flow to weather. Dept. of Met., MIT, Final Rep.

Sawyer, J. S., 1959: The introduction of the effects of topography into methods of numerical forecasting. *Quart. J. Roy. Meteor. Soc.*, 85, 31-43.

Schmidt, P. J., and D. R. Johnson, 1972: Use of approximating polynomials to estimate profiles of wind, divergence and vertical motion. *Mon. Wea. Rev.*, 100, 345-353

Shuman, F. G., 1957: Numerical methods in weather prediction: II Smoothing and filtering. *Mon. Wea. Rev.*, 85, 11, 357-361.

Smith, P. J., 1971: An analysis of kinematic vertical motions *Mon. Wea. Rev*, 99, 10, 715-724

Sutton, O. G., 1953: *Micremteorology.* McGraw Hill Book Co

垂直速度之合成個案研究

陳 泰 然

國立臺灣大學大氣科學系

摘 要

本文引用一特殊糾正方法來間接評估垂直速度之三度空間分佈情形。冬季寒潮爆發，實爲低緯度一重要之天氣現象，因而選用了四個冬季寒潮爆發個案，引用 O'Brien (1970) 之方法對其合成之高低氣壓做分析，結果顯示最大上升下降速度發生地區有別於其他非寒潮爆發之個案研究。對於水平及垂直方面之垂直速度分佈以及雷達觀測報告均以圖分析並加討論。